Identification of LIMK2 as a Therapeutic Target in Castration Resistant Prostate Cancer

Kumar Nikhil[1], Lei Chang[1], Keith Viccaro[1], Max Jacobsen[2], Callista McGuire[2], Shakti R. Satapathy[1], Michael Tandiary[1], Meaghan M. Broman[3], Gregory Cresswell[3], Yizhou J. He[4], George E. Sandusky[2], Timothy L Ratliff[3], Dipanjan Chowdhury[4], Kavita Shah[1]*

[1.] Department of Chemistry and Purdue University Center for Cancer Research

560 Oval Drive, West Lafayette, IN 47907

Email: shah23@purdue.edu

[2.] Department of Pathology and Laboratory Medicine, Indiana University School of Medicine

635 Barnhill Drive, room A-128, Indianapolis, IN 46202

[3.] Department of Comparative Pathobiology and Purdue University Center for Cancer Research

625 Harrison Street, West Lafayette, IN 47907

[4.] Dana Farber Cancer Institute, Harvard Institute of Medicine, Room HIM-229, 4 Blackfan Cir.

Boston, MA 02215

***** To whom correspondence should be addressed

Keywords: LIMK2, TWIST1, Castration resistant prostate cancer, Prostate cancer

List of abbreviations: LIMK2: LIMK Kinase 2; CRPC: Castration resistant prostate cancer; ADT: androgen-deprivation therapy; AR: androgen receptor; CR: castration resistant; ORF: open reading frame.

This is the author's manuscript of the article published in final edited form as:

Nikhil, K., Chang, L., Viccaro, K., Jacobsen, M., McGuire, C., Satapathy, S. R., … Shah, K. (2019). Identification of LIMK2 as a Therapeutic Target in Castration Resistant Prostate Cancer. Cancer Letters. https://doi.org/10.1016/j.canlet.2019.01.035

Abstract

This study identified LIMK2 kinase as a disease-specific target in castration resistant prostate cancer (CRPC) pathogenesis, which is upregulated in response to androgen deprivation therapy, the current standard of treatment for prostate cancer. Surgical castration increases LIMK2 expression in mouse prostates due to increased hypoxia. Similarly, human clinical specimens showed highest LIMK2 levels in CRPC tissues compared to other stages, while minimal LIMK2 was observed in normal prostates. Most notably, inducible knockdown of LIMK2 fully reverses CRPC tumorigenesis in castrated mice, underscoring its potential as a clinical target for CRPC. We also identified TWIST1 as a direct substrate of LIMK2, which uncovered the molecular mechanism of LIMK2-induced malignancy. TWIST1 is strongly associated with CRPC initiation, progression and poor prognosis. LIMK2 increases TWIST1 transcription upon hypoxia; and stabilizes TWIST1 by direct phosphorylation. TWIST1 also stabilizes LIMK2 by inhibiting its ubiquitylation. Phosphorylation-dead TWIST1 acts as dominant negative and fully prevents EMT and tumor formation *in vivo*, thereby highlighting the significance of LIMK2-TWIST1 signaling axis in CRPC. As LIMK2 null mice are viable, targeting LIMK2 should have minimal collateral toxicity, thereby improving the overall survival of CRPC patients.

Highlights:

• LIMK2 was identified as a disease-specific target in CRPC.

• We show that LIMK2 is upregulated in castrated prostates due to increased hypoxia.

• Inducible knockdown of LIMK2 fully reverses CRPC tumorigenesis in castrated mice.

• TWIST1 was identified as a direct target of LIMK2.

• LIMK2 inhibitor shows very high synergy with docetaxel.

Running Title: Multifaceted Regulation of TWIST1 by LIMK2 in CRPC

Abstract

This study identified LIMK2 kinase as a disease-specific target in castration resistant prostate cancer (CRPC) pathogenesis, which is upregulated in response to androgen deprivation therapy, the current standard of treatment for prostate cancer. Surgical castration increases LIMK2 expression in mouse prostates due to increased hypoxia. Similarly, human clinical specimens showed highest LIMK2 levels in CRPC tissues compared to other stages, while minimal LIMK2 was observed in normal prostates. Most notably, inducible knockdown of LIMK2 fully reverses CRPC tumorigenesis in castrated mice, underscoring its potential as a clinical target for CRPC. We also identified TWIST1 as a direct substrate of LIMK2, which uncovered the molecular mechanism of LIMK2-induced malignancy. TWIST1 is strongly associated with CRPC initiation, progression and poor prognosis. LIMK2 increases TWIST1 mRNA levels upon hypoxia; and stabilizes TWIST1 by direct phosphorylation. TWIST1 also stabilizes LIMK2 by inhibiting its ubiquitylation. Phosphorylation-dead TWIST1 acts as dominant negative and fully prevents EMT and tumor formation *in vivo*, thereby highlighting the significance of LIMK2-TWIST1 signaling axis in CRPC. As LIMK2 null mice are viable, targeting LIMK2 should have minimal collateral toxicity, thereby improving the overall survival of CRPC patients.

1. Introduction

Prostate cancer (PCa) ranks second in terms of cancer-related deaths among men in the US [1]. The primary cause is the emergence of castration-resistant prostate cancer (CRPC), and subsequent metastasis and chemoresistance for which there is no known cure [2]. Early stage prostate tumors can be treated by surgery, radiation, and/or androgen-deprivation therapy (ADT). Treatment failure typically occurs within 2-3 years in almost all patients, giving rise to CRPC. Second generation ADT agents, abiraterone and enzalutamide, and docetaxel or cabazitaxel based chemotherapy regimens are next in line treatments, however, CRPC tumors are either intrinsically resistant or rapidly develop resistance to these agents, causing fatality in vast majority of patients. Therefore, an urgent need exists to identify specific molecular targets that prevent the emergence of CRPC or selectively abrogate castration-resistant (CR) tumors, and/or render these tumors highly sensitive to chemotherapy, thereby improving overall survival in patients.

This study focuses on LIM-domain kinase-2 (LIMK2) as a potential clinical target for the prevention and treatment of CRPC. LIMK2 regulates actin dynamics in normal cells [3, 4]. LIMK2 promotes metastasis in fibrosarcoma, and metastasis and angiogenesis in pancreatic cancer [5, 6]. We have demonstrated that LIMK2 is a crucial oncogenic regulator and effector of Aurora A kinase (AURKA) in breast cancer [7]. AURKA and LIMK2 positively regulate each other's protein levels, triggering a feedback loop that promotes oncogenesis. Although LIMK2 has not been explored as a therapeutic target in PCa, AURKA is overexpressed in 96% of high-grade prostate intraepithelial neoplasia and 98% of PCa lesions [8, 9]. AURKA is also significantly overexpressed in CRPC [10], suggesting that LIMK2 may be concurrently expressed in these tissues. AURKA inhibition sensitizes CRPC cells to radiation, underscoring

its critical role in CRPC [11]. Despite these encouraging findings, AURKA inhibition in Phase II clinical trials has been associated with several adverse side effects, suggesting that collateral inhibition of AURKA in rapidly proliferating normal tissues is responsible for the undesirable side effects. These findings indicate that selective targeting of oncogenic targets of AURKA in PCa may be a superior option for developing effective drugs and combating collateral toxicity. To this end, we identified LIMK2 as a highly oncogenic target of AURKA, ablation of which completely abrogates tumorigenesis in nude mice [7]. Importantly, unlike AURKA, LIMK2 null mice are viable [12], suggesting that LIMK2 inhibition should cause minimal collateral toxicity in patients.

2. Materials and Methods

2.1. Antibodies

Validated antibodies against LIMK2, Actin, and TWIST1 were purchased from Santa Cruz Biotech (Santa Cruz, CA). Snail, Slug, N-cadherin and CD44 antibodies were purchased from One World Lab (San Diego, CA). Antibodies against Vimentin, E-cadherin and MMP-2 were purchased from Bioss (Woburn, MA). All antibodies are validated and were used at 1-1000 dilution. Antibody details are provided in Supplementary Table 1.

2.2. LIMK2 and TWIST1 shRNAs

LIMK2 shRNAs in pLKO vector were generated in our previous study [7]. The sequences and vectors of inducible LIMK2 shRNAs and TWIST1 shRNAs are provided in Supplementary information (section 2) and Supplementary Table 2.

2.3. In vitro Kinase Assays

Kinase assays were conducted as described before [14]. The details are included in Supplementary section 4.

2.4. Immunofluorescence

Immunofluorescence is described in Supplementary section 6 [15].

2.5. Semi-quantitative PCR and Real-Time qPCR

The details are included in Supplementary section 7 and Supplementary Table 3.

2.6. Immunohistochemistry

The protocol is included in Supplementary section 8.

2.7. LIMK2 Reporters and Luciferase Assay

The generation of LIMK2-luciferase plasmids and reporter assay is included in Supplementary section 9.

2.8. Prostatosphere Assay, Soft agar colony formation, Ubiquitylation, Chemotaxis and MTT assays

These assays were conducted as reported before [16-24]. The details are included in Supplementary sections 10-14.

2.9. LIMK2 CRISPR plasmid and LIMK2 CRISPR C4-2 cell line

The details are included in Supplementary sections 15.

2.10. *In vivo* xenograft in nude mice:

The details are included in Supplementary sections 16. Animal care was in accordance with institution guidelines.

Statistical analysis

Data are expressed as mean±s.e.m. and were statistically evaluated with oneway ANOVA followed by the Bonferroni post hoc test using GraphPad Prism 5.04 software (GraphPad Software). $P<0.05$ was considered statistically significant.

3. Results

3.1. LIMK2 levels increase upon castration in mice

It would be ideal to target an oncogenic driver of CRPC that is specifically upregulated by cancer cells in response to ADT, the current standard of treatment. Therefore, we analyzed how LIMK2 levels might be modulated upon castration in mice. LIMK2 levels were analyzed in mouse prostates on different days post-castration. LIMK2 levels steadily increased after castration with

~4-fold increase on day 7 (Figure 1A). We also investigated IL-6 level (positive control), which is increased in untreated CRPC patients compared with healthy controls or patients with localized disease [25, 26]. Figure 1B shows average LIMK2 and IL6 levels from three mice for every time point.

We further examined LIMK2 levels using immunohistochemistry in prostate tissues isolated from mice on day 0, 5, 14 and 28 days post-castration. LIMK2 levels increased steadily in castrated prostates with significantly high levels after 14 days, confirming that LIMK2 increases upon castration (Figure 1C).

3.2. LIMK2 is a direct target of hypoxia

Castration in non-malignant prostate tissues increases hypoxia [27-30]. Thus, we investigated whether LIMK2 is upregulated due to hypoxia. Initially, we used cobalt chloride ($CoCl_2$) to mimic hypoxia in castration-resistant C4-2 cells [31], which resulted in ~2-fold increase in LIMK2 levels. As a positive control, TWIST1 was analyzed, which increases upon hypoxia [32]. TWIST1 levels also increased ~2-fold upon exposure to $CoCl_2$ (Figure 1D, 1E).

LIMK2 protein was next analyzed in hypoxia-exposed C4-2 cells, which confirmed a 2-3-fold increase in LIMK2 and TWIST1 levels (Figures 1F, 1G). To determine whether this upregulation was due to increased LIMK2 mRNA levels, we measured them using real-time qPCR in hypoxia-exposed cells, which revealed a 2-fold increase in 18h (Figure 1H). Increase in TWIST1 mRNA levels upon hypoxia served as the positive control.

We next generated four luciferase reporter constructs containing genomic fragments upstream from the *LIMK2* open reading frame (-360, -600, -900 and -1038). Exposure of C4-2

cells to 100 μM $CoCl_2$ triggered significant increase in LIMK2 promoter luciferase activity. Particularly, pGL3-600 luc-plasmid showed >7-fold increase after 24h (Figure 1I), indicating that $CoCl_2$ activates LIMK2 promoter. LIMK2 promoter activity was subsequently examined in hypoxia-treated cells, which also revealed robust activation (Figure 1J). To further examine whether LIMK2 upregulation was HIF1α or HIF2α-dependent, we ectopically expressed these proteins, which resulted in strong upregulation of LIMK2 (Supplementary Figure 1A). Together, these results strongly support that hypoxia increases LIMK2 levels. As castration leads to hypoxia, we postulate that increased hypoxia is one of the mechanisms by which LIMK2 is upregulated upon castration.

We next examined whether LIMK2 levels are regulated upon androgen-deprivation in cells. Androgen-sensitive LNCaP cells were exposed to charcoal-stripped androgen-deprived media for 12h, which did not change LIMK2 levels significantly (Figure 1K, 1L). This is presumably because tissue culture cells do not experience hypoxia under regular growth conditions despite androgen depletion, further indicating that hypoxia is a key mechanism that upregulates LIMK2 upon androgen depletion in vivo.

3.3. LIMK2 increases TWIST1 mRNA levels under hypoxic conditions

LIMK2 has not been linked to hypoxia. Thus, we investigated whether LIMK2 and TWIST1 regulate each other mRNA levels under normoxia and/or hypoxia. Surprisingly, LIMK2 depletion using LIMK2 shRNA decreased *TWIST1* mRNA levels under hypoxia, but not under normoxia (Figure 2A). In contrast, TWIST1 protein was significantly reduced both under

hypoxia and normoxia upon LIMK2 ablation, indicating LIMK2 regulates TWIST1 protein also (Figures 2B, 2C).

To validate these results, we generated LIMK2 knockout C4-2 cells using CRISPR and analyzed *TWIST1* transcript levels. LIMK2 knockout decreased *TWIST1* levels significantly under hypoxia, although a marginal decrease was also observed under normoxia, which was statistically insignificant (Figure 2D). As before, TWIST1 protein was significantly decreased both under normoxia and hypoxia in LIMK2 knockout cells (Figure 2E, F), confirming that LIMK2 upregulates TWIST1 both at mRNA and protein levels.

3.4. TWIST1 does not regulate LIMK2 mRNA levels

To investigate whether TWIST1 regulates LIMK2 mRNA levels in a feedback mechanism, we ablated TWIST1 under normoxic and hypoxic conditions, which revealed minimal changes in *LIMK2* mRNA levels (Figure 2G). We also analyzed LIMK2 protein in TWIST1-ablated cells under normoxia and hypoxia. Interestingly, TWIST1 ablation decreased LIMK2 protein under normoxia (Figure 2H, I), indicating that TWIST1 does not regulate *LIMK2* mRNA levels, but regulates LIMK2 protein.

3.5. LIMK2 expression increases with disease progression in PCa clinical specimens

LIMK2 has not been analyzed in PCa tissues. We analyzed LIMK2 levels in normal prostate (n = 8), benign prostatic hyperplasia (n = 16), localized PCa (n = 13) and CRPC tissues (n = 7) obtained from biopsy from IU Pathology Archives. Additionally, we analyzed LIMK2 levels in a prostatic carcinoma TMA containing 92 cores and PCa clinical specimens obtained from CHTN

bank (20 specimens). In normal prostate and stage II tissues, minimal LIMK2 was present (Figure 3A). In stage 3 PCa tissues, some stromal LIMK2 immunostaining was detected. The immunostaining was seen as positive brown staining (localized to stroma) surrounding the islands composed of tightly packed back to back small glands of PCa. The distribution of hand count staining was as follows: no staining 0, mild staining 3-6, moderate staining 7-14, and strong staining 14-28. Stage III and IV were moderate to strong strainers, while stage I and II had zero to moderate staining (Figure 3B). Importantly, CRPC cases exhibited strong epithelial and stromal staining compared to the other groups (>95% cases). Together, these results show LIMK2 is minimally present in normal prostates; however, its upregulation occurs early in PCa progression and increases with disease severity. Furthermore, LIMK2 is significantly upregulated in the epithelial cells and stroma of CRPC tissues.

3.6. Inducible LIMK2 knockdown reverses tumorigenesis in mice

Castration increased LIMK2 levels in mice. Further, LIMK2 expression was highest in CRPC specimens. Therefore, we determined whether LIMK2 knockdown affects tumorigenesis in castrated mice. We generated two inducible LIMK2 shRNAs expressing C4-2 cells, each of which contained a different shRNA in a different inducible vector (Tet-pLKO.1 and LT3GEPI, 33 and Supplementary Table 2). Both of these cell lines expressed similar levels of LIMK2 as compared to control C4-2 cells in the absence of doxycycline (Figure 3B). Doxycycline treatment for 48h resulted in >90% knockdown in both LIMK2-shRNA containing cells, with no effect in control cells. These results show that Tet-pLKO.1-LIMK2 shRNA and LT3GEPI-LIMK2 shRNA containing cells specifically and potently downregulate LIMK2 in a doxycycline-inducible manner (Figure 3B).

These cells along with control cells were subcutaneously injected on the shoulders of castrated nude mice (n=3 for each group). All cell lines exhibited similar tumorigenic potential and formed similar size tumors. On day 24, each set of mice showed ~1500 mm^3 tumor size, at which point doxycycline treatment was initiated in all three sets. Inducible knockdown of LIMK2 in Tet-pLKO.1-LIMK2 shRNA and LT3GEPI-LIMK2 shRNA xenografts caused a rapid and potent regression of tumors in all mice, whereas C4-2 xenografts increased rapidly as time progressed (Figure 3C, D). All sets of mice were euthanized on day 45. C4-2 xenografts formed larger than 2800 mm^3 tumors, whereas in LIMK2 knockdown xenografts, the tumor regressed from a size of 1500 mm^3 to less than 100 mm^3 (Figure 3D, E). These results strongly support the therapeutic potential of LIMK2 as a clinical target for CRPC.

3.7. TWIST1 is a direct LIMK2 substrate

The robust reversal of tumorigenesis observed upon LIMK2 downregulation prompted us to investigate the molecular mechanism by which it promotes oncogenesis. To date, cofilin, and MT1-MMP are the only known LIMK2 substrates. LIMK2 regulates actin dynamics via cofilin [3]. LIMK2 regulates tumor growth and cell migration through MT1-MMP phosphorylation in breast cancer cells [34]. LIMK2-mediated upregulation of TWIST1 mRNA encouraged us to investigate whether it also regulates TWIST1 post-translationally via phosphorylation. TWIST1 upregulation is strongly associated with CRPC initiation and progression [35, 36]. We generated 6x-His-TWIST1 and subjected it to a kinase assay. LIMK2 directly phosphorylated TWIST1, indicating that LIMK2 also regulates TWIST1 post-translationally (Figure 4A).

3.8. LIMK2 phosphorylates TWIST1 at four sites

Protein kinases predominantly recognize and phosphorylate their substrates by docking interactions and the linear consensus motif near the phosphosite [37, 38]. A recent study showed that LIMK1 (LIMK2 family member) recognizes cofilin by docking interactions, but does not have extensive interactions with cofilin near the phosphosite [39]. This conclusion is supported by another study, which revealed no optimal sequence specificity for LIMK1 in a peptide array screening [40]. LIMK2 peptide specificity has not been analyzed. LIMK2 phosphorylates cofilin and ADF at Ser3, which is followed by an alanine. Therefore, we initially focused on all Ser residues on TWIST1 that were followed by either an alanine or a glycine. We chose five putative sites as potential LIMK2 sites (S31, S45, S78, S95 and S199) on TWIST1 and generated the corresponding phosphorylation-dead single mutants. Among these, S45, S78, S95 and S199 were phosphorylated by LIMK2 (Figure 4B, C). In contrast, S31A-TWIST1 mutant showed no reduction in phosphorylation compared with wild-type (WT) TWIST1, suggesting this site is not phosphorylated by LIMK2 (data not shown). Furthermore, the corresponding phosphorylation-dead quadruple mutant (denoted as 4A) was not phosphorylated by LIMK2, confirming that S45, S78, S95 and S199 are the only LIMK2 sites on TWIST1 (Figure 4D).

3.9. LIMK2 does not regulate TWIST1 subcellular localization

We observed that LIMK2 was predominantly cytoplasmic with some nuclear localization, whereas TWIST1 was mainly nuclear in C4-2 cells (Supplementary Figures 1B and 1C respectively). LIMK2 knockdown did not affect TWIST1 localization (Figure 4E). We also stably expressed WT and phospho-dead 4A-TWIST1 in C4-2 cells and analyzed their subcellular localization using HA antibody, both of which exhibited similar localization as endogenous

TWIST1 (Figure 4F, G). These results were further confirmed using subcellular fractionation, which confirmed that LIMK2 does not affect the subcellular localization of TWIST1 (Figure 4H).

3.10. LIMK2 positively regulates TWIST1 protein levels

LIMK2 overexpression increased, and LIMK2 knockdown decreased TWIST1 levels both in C4-2 (Figure 5A-D) and 22Rv1 cells (Supplementary Figure 1D, E). As LIMK2 increases TWIST1 mRNA levels, these results were expected. Therefore, to investigate whether LIMK2 regulates TWIST1 post-translationally, we generated LIMK2-C4-2 cells, exposed them to cycloheximide to prevent further protein synthesis, and analyzed TWIST1 degradation profile. LIMK2 overexpression reduced TWIST1 degradation, indicating that LIMK2 regulates TWIST1 protein (Figures 5E-G). We also expressed 6x-His-ubiquitin in C4-2 and LIMK2-depleted-C4-2 cells, and analyzed the ubiquitylation of TWIST1. LIMK2 knockdown led to increased TWIST1 ubiquitylation (Figure 5H), thus confirming that LIMK2 stabilizes TWIST1 levels by inhibiting its ubiquitin-mediated degradation.

3.11. LIMK2 prevents TWIST1 degradation via phosphorylation

To examine whether LIMK2-mediated phosphorylation of TWIST1 prevents its degradation, WT and 4A-TWIST1 were stably expressed in C4-2 cells and their levels analyzed. WT TWIST1 levels were significantly higher compared to 4A-TWIST1, suggesting that LIMK2-mediated phosphorylation of TWIST1 stabilizes it (Figure 5I).

We next examined whether 4A-TWIST1 was resistant to LIMK2-mediated protein stabilization. We transiently depleted LIMK2 from TWIST1-C4-2 and 4A-TWIST1-C4-2 cells and analyzed their relative ubiquitylation. While WT-TWIST1 was significantly ubiquitylated upon LIMK2 depletion, 4A-TWIST1 showed little ubiquitylation suggesting that LIMK2-mediated phosphorylation stabilizes TWIST1 (Figure 5J).

To determine the individual contribution of each of the phosphorylation site to protein stabilization, we infected HA-tagged WT and phospho-dead single mutants of TWIST1 in C4-2 cells and examined their levels. While S45A level was slightly reduced compared to WT, S75A, S96A and S199A mutants displayed much reduced protein levels (Figures 5K, 5L). We confirmed these findings by examining the ubiquitylation of each of the single mutant ± LIMK2 depletion. As expected, S45A-TWIST1 showed slightly less ubiquitylation compared to WT, whereas other mutants were significantly less ubiquitylated upon LIMK2 depletion, indicating that phosphorylation of TWIST1 increases its stability (Figure 5M).

3.12. TWIST1 positively regulates LIMK2 protein

TWIST1 depletion under normoxia decreases LIMK2 protein but not its mRNA (compare Figures 2G and 2H). Similarly, 4A-TWIST1 expressing cells revealed significantly lower LIMK2 compared to control C4-2 and WT-TWIST1-C4-2 cells (Figure 5K), suggesting that TWIST1 regulates LIMK2 protein. Thus, we overexpressed TWIST1, which increased LIMK2 levels (Figure 6A, B) and TWIST1 knockdown significantly decreased LIMK2 levels (Figure 6C, D). Similar results were obtained in 22Rv1 cells, confirming the feedback loop between TWIST1 and LIMK2 (Supplementary Figure 2A, B).

We examined whether TWIST1 increases LIMK2 levels by inhibiting its degradation. TWIST1 overexpression significantly reduced LIMK2 degradation in cycloheximide-treated cells, confirming that TWIST1 stabilizes LIMK2 (Figures 6E-G). We further observed increased ubiquitylation of LIMK2 upon TWIST1 depletion (Figure 6H), indicating that TWIST1 increases LIMK2 levels by preventing its degradation thereby eliciting a positive feedback loop.

3.13. TWIST1 and LIMK2 feedback loop promotes aggressive cancer phenotypes

Ectopic expression of either LIMK2 or TWIST1 increased cellular proliferation (Figure 7A). In contrast, expression of 4A-TWIST1 significantly inhibited cell proliferation, which was lower than C4-2 cells. In addition, LIMK2 depletion substantially reduced, and its overexpression significantly increased proliferation in TWIST1-C4-2 cells, but not in 4A-TWIST1-C4-2 cells. These results indicate that the TWIST1-mediated increase in cell proliferation is predominantly due to LIMK2-mediated phosphorylation (Figures 7B, 7C). Similar results were obtained in 22Rv1 cells, where LIMK2 knockdown decreased, and its overexpression increased cell proliferation in 22Rv1 and TWIST1-22Rv1 cells, but not in 4A-TWIST1-22Rv1 cells (Supplementary Figures 3A-C). These results show that LIMK2-mediated phosphorylation of TWIST1 contributes significantly to increased cell proliferation.

The effect of TWIST1 phosphorylation was also examined under anchorage-independent conditions. TWIST1 expression considerably increased colony formation in C4-2 and 22Rv1 cells, compared to control cells (Figure 7D and Supplementary Figure 3D, respectively). In contrast, 4A-TWIST1 acted as dominant negative and exhibited minimal number of colonies, indicating that LIMK2-mediated phosphorylation of TWIST1 promotes cell proliferation both under attached and anchorage-independent conditions.

3.14. TWIST1 and LIMK2 feedback loop increases cell migration

TWIST1 overexpression led to a robust increase in cell motility as expected (Figure 7E, F). By contrast, 4A-TWIST1 overexpression considerably impaired chemotaxis compared to C4-2 cells, confirming that 4A-TWIST1 acts as dominant-negative and inhibits cell motility. Similarly, LIMK2 knockdown decreased; and its overexpression increased cell motility in TWIST1-C4-2 cells, but not in 4A-C4-2 cells (Figures 7G-J) and 22Rv1 cells (Supplementary Figure 3E-J). These results corroborate that LIMK2-mediated phosphorylation of TWIST1 is crucial for cell motility in CRPC cells.

3.15. LIMK2 promotes Epithelial-to-mesenchymal Transition (EMT) via TWIST1

EMT and cancer stem cells (CSCs) play crucial roles during the development of CRPC [41]. Castration can cause EMT, which increases the stemness of CSCs, leading to metastasis. TWIST1 is a key driver for EMT and drug resistance. We thus examined whether LIMK2 knockdown inhibits EMT and CSC. TWIST1 expression downregulates E-cadherin, an epithelial marker, but upregulates mesenchymal markers N-cadherin, CD44, Slug and Snail [42, 43].

Ectopic expression of TWIST1 decreased E-cadherin, but increased the EMT markers as expected (Figure 7K). 4A-TWIST1 not only prevented the increase in EMT markers, it displayed even lower levels than parental cells. In addition, 4A-TWIST1 expression increased E-cadherin level, further confirming that LIMK2-mediated phosphorylation plays a crucial role in TWIST1-mediated EMT phenotype.

We also conducted a sphere-forming assay to measure the self-renewal capacity of C4-2, TWIST1-C4-2 and 4A-TWIST1-C4-2 cells. CSCs grow in suspension under ultra-low attachment conditions and form independent spheres. When subjected to these conditions, C4-2 formed aggregates of cells but no prostatosphere formation (Figure7L). In contrast, TWIST1 overexpression induced large prostatosphere formation. 4A-TWIST1-C4-2 cells showed no prostatosphere formation either, thereby confirming that LIMK2-mediated phosphorylation of TWIST1 contributes to CSC phenotype.

3.16. Significance of TWIST1 phosphorylation in drug resistance and cell viability

As EMT contributes to drug resistance, we examined doxorubicin sensitivity in C4-2 cells, and observed ~40% loss in cell viability in 24h. TWIST1 expression offered resistance to doxorubicin (~20% loss), whereas 4A-TWIST1 expression rendered these cells highly sensitive to doxorubicin -induced toxicity (~57% loss) (Figure 7M). Thus, concurrent inhibition of LIMK2 and TWIST1 may act synergistically in targeting highly chemoresistant CRPC.

3.17. LIMK2-mediated TWIST1 phosphorylation is crucial for tumorigenesis *in vivo*

Male nude mice were subcutaneously inoculated with C4-2 and TWIST1-C4-2 cells on the left and right shoulders, respectively. While TWIST1-C4-2 cells formed robust tumors, C4-2 cells displayed very small tumor formation (Fig. 8A, B). To investigate the contribution of LIMK2-mediated phosphorylation, we also subcutaneously inoculated another set of nude mice with TWIST1-C4-2 cells and 4A-TWIST1-C4-2 cells on right and left shoulders, respectively. While TWIST1-C4-2 cells formed robust tumors, 4A-TWIST1-C4-2 cells showed absolutely no tumor

formation (Fig. 8C, D). These results confirm that phosphorylation of TWIST1 by LIMK2 is crucial for its tumorigenic potential *in vivo.*

3.18. TWIST1-C4-2 xenografts express high levels of EMT markers

We further examined the levels of E-cadherin and EMT markers in C4-2 and TWIST1-C4-2 xenografts. As 4A-TWIST1-C4-2 cells did not form any tumor, they could not be analyzed *in vivo*. One-half of the tumor was snap-frozen for immunoblot analysis and other half was used to generate paraffin-embedded slides for immunohistochemistry. E-cadherin levels were lower in TWIST1-C4-2 xenograft, compared to C4-2 xenografts (Figure 8E, F). In contrast, LIMK2, N-cadherin, Vimentin, MMP-2, CD44, Slug and Snail levels were significantly higher in TWIST1-C4-2 compared to C4-2 xenograft. Increase in LIMK2 levels in TWIST1 xenograft further confirms the feedback loop *in vivo*.

The immunohistochemistry data supported the immunoblot findings and exhibited robust expression of LIMK2, CD44, MMP2, Slug and Snail in TWIST1 overexpressing xenografts, compared to parental cells xenograft. Similarly, E-cadherin was absent in TWIST1-C4-2 xenografts, but abundantly expressed in C4-2 xenografts (Figure 8G-L). These findings further confirm that TWIST1 promotes EMT in CRPC cells *in vivo*.

3.19. LIMK2 Inhibition shows high synergy with Docetaxel

Docetaxel is the first line treatment for CRPC, however, these tumors rapidly develop resistance to chemotherapy. We investigated whether LIMK2 inhibition sensitizes CRPC cells to docetaxel. We synthesized an allosteric LIMK2 inhibitor (LI) (IC_{50} 39 nM), which shows 100-fold

selectivity over its closest relative LIMK1 [44]. C4-2 cells were treated with varying doses of LI and docetaxel for 48h and cell death analyzed. When either 10 nM docetaxel or 10 μM LI was used, 2-3% cell death was observed, which increased to ~7% when they were used in combination (Figure 8M). However, when cells were pre-treated with docetaxel for 12h, followed by LI treatment, it showed extremely high synergy (combination-index of 0.15), indicating that LIMK2 inhibition should be highly effective in sensitizing CRPC cells to docetaxel-induced therapy.

4. Discussion

LIMK2 upregulation and activation occurs in several cancers [6, 7, 45-49]. TGFβ and bone morphogenetic protein receptor-2 activate LIMK2 by Rho/ROCK pathway [49, 50]. In SCLC, a long non-coding RNA-TUG1 regulates the expression of LIMK2b (a splice variant), which leads to cell growth and chemoresistance [51]. However, the downstream substrates by which LIMK2 promotes tumorigenesis, metastasis, chemoresistance and angiogenesis remain unknown. LIMK2's levels or its role in PCa has not been analyzed to date.

This study revealed that LIMK2 is upregulated upon castration in mice. This finding was supported by human clinical prostate tissues analysis, which showed negligible expression in normal prostates, but the levels increase with disease severity, with the highest levels in CRPC. Notably, the significance of LIMK2 as a potential clinical target was shown by its inducible knockdown, which fully reversed tumorigenesis in nude mice. These findings strongly underscore a key role of LIMK2 in promoting CRPC pathogenesis.

We identified hypoxia as a key mechanism that leads to LIMK2 upregulation. ADT exacerbates hypoxic stress in PCa, which subsequently promotes androgen receptor (AR)-dependent and independent pathways leading to CRPC [52, 53]. Tumor-hypoxia is associated with increased angiogenesis, metabolic reprogramming, EMT, metastasis, CSC phenotype, immune evasion, and resistance to chemotherapy and radiation therapy [54]. Thus, hypoxia is associated with poor prognosis in CRPC [55, 56]. Our data suggest that LIMK2 upregulation triggered by hypoxia contributes to aggressive oncogenic phenotypes in CRPC.

We further identified TWIST1 as a direct LIMK2 substrate. TWIST1 is essential for embryonic development and organogenesis. Postnatally, TWIST1 expression is limited to quiescent adult stem cells located in mesenchymal tissues. Repeated neoadjuvant chemotherapy triggers TWIST1 upregulation, which correlates with extreme chemoresistance [57]. TWIST1 is upregulated following ADT in PCa tissues [58], which causes AR transcription, chemoresistance and invasion [34, 59]. Thus, our finding identifying LIMK2 as both an upstream regulator and a downstream effector of TWIST1 has significant implications for CRPC therapy (Figure 8N).

Acquisition of drug-resistance and metastatic phenotype via EMT are both critical steps towards the progression of CRPC. ADT increases TGFβ signaling (18), which promotes TWIST1 and AR expression, causing EMT and PCa growth [60]. As TGFβ activates LIMK2, we postulate that TGFβ-mediated increase in LIMK2 activity may be critical for subsequent increase in TWIST1 levels in CRPC. We show that LIMK2-mediated phosphorylation of TWIST1 and its subsequent stabilization is one of the vital mechanisms by which EMT phenotype is acquired in CRPC. 4A-TWIST1 mutant acts as dominant-negative, which decreases the levels of endogenous TWIST1 in cells, which in turn reduces LIMK2 levels due to the positive feedback loop (Figure 5I). Accordingly, 4A-TWIST1 expression reverses EMT and CSC phenotypes in

CRPC cells (Figure 7K). This finding is further strengthened by *in vivo* data, showing the incompetency of 4A-TWIST1 cells to form any tumors in mice.

LIMK2 and TWIST1 are involved in a reciprocal feedback loop, where each stabilizes the other's protein level. This finding is important for two reasons: first, LIMK2 inhibition provides a potent tool to reduce TWIST1 levels, which is highly desirable for CRPC prevention and therapy. Second, the reciprocal loop between TWIST1 and LIMK2 ensures that their concurrent inhibition will be highly synergistic in inhibiting CRPC tumorigenesis, chemoresistance and metastasis.

In summary, this study reveals the oncogenic potential of LIMK2 as a prospective clinical target in CRPC. We postulate that targeting LIMK2 will likely be beneficial in inhibiting PCa, including its progression towards CRPC. LIMK2 null mice are viable suggesting that targeting LIMK2 will have minimal collateral toxicity. Also, LIMK2 inhibition is expected to sensitize CRPC tumors to chemotherapy, improving overall survival of CRPC patients.

Authors Contributions:

KN conducted most of the cell, tissue IHC and animal experiments. LC contributed Fig. 5A, 5H, 6A and 6E-H. KV generated TWIST1 mutants and conducted kinase assays (Fig. 4A, B, D); MJ and CM conducted IHC in human specimens (Figure 3); SRS generated inducible LIMK2-shRNA C4-2 cells; MT synthesized LIMK2 inhibitor; MMB provided castrated mouse prostate slides; GC helped with hypoxia experiments; YJH generated pLenti-CRISPR-v3.1 vector; GES supervised and analyzed IHC data; GES, DC and TLR provided critical input for the manuscript; KS conceived the idea and wrote the manuscript with input from all authors.

5. Acknowledgements

This work was supported by U.S. Army Medical Research Acquisition Activity, Prostate Cancer Research Program (Award # PC130391 to KS). KS also gratefully acknowledges the Biological Evaluation facility, particularly Dr. Ben Elzey and support from the Purdue University Center for Cancer Research (NIH grant P30 CA023168) for *in vivo* experiments (Figures 8A, B). We thank Dr. Johannes Zuber for LT3GEPIR plasmid. pLKO.1 TRC vector was a gift from David Root (Addgene plasmid # 10878) [61] and Tet-pLKO-puro was a gift from Dmitri Wiederschain (Addgene plasmid # 21915) [62]. plentiCRISPR v2 was a gift from Feng Zhang (Addgene plasmid # 52961) [63].

6. Conflict of Interest

The authors declare no conflict of interest.

References

1. Stavridi F, Karapanagiotou EM, Syrigos KN. Targeted therapeutic approaches for hormone-refractory prostate cancer. Cancer Treat Rev. 2010:36(2):122-30.
2. Lassi K, Dawson NA. Drug development for metastatic castration-resistant prostate cancer: current status and future perspectives. Future Oncol. 2011:7(4):551-8.

3. Sumi T, Matsumoto K, Takai Y, Nakamura T. Cofilin phosphorylation and actin cytoskeletal dynamics regulated by rho- and Cdc42-activated LIM-kinase 2. J. Cell Biol. 1999;147:1519-1532.

4. Sumi T, Matsumoto K, Nakamura T. Specific activation of LIM kinase 2 via phosphorylation of threonine 505 by ROCK, a Rho-dependent protein kinase. J. Biol. Chem. 2001;276:670-676.

5. Suyama E, Wadhwa R, Kawasaki H, Yaguchi T, Kaul SC, Nakajima M, et al. LIM kinase-2 targeting as a possible anti-metastasis therapy. J Gene Med. 2004;6(3):357-63.

6. Vlecken DH, Bagowski CP. LIMK1 and LIMK2 are important for metastatic behavior and tumor cell-induced angiogenesis of pancreatic cancer cells. Zebrafish. 2009;6(4):433-9.

7. Johnson EO, Chang KH, Ghosh S, Venkatesh C, Giger K, Low PS et al. LIMK2 is a crucial regulator and effector of Aurora-A-kinase-mediated malignancy. J Cell Sci. 2012;125:1204-16.

8. Lee EC, Frolov A, Li R, Ayala G, Greenberg NM. Targeting Aurora kinases for the treatment of prostate cancer. Cancer Res. 2006;66(10):4996-5002.

9. Buschhorn HM, Klein RR, Chambers SM, Hardy MC, Green S, Bearss D, *et al*. Aurora-A over-expression in high-grade PIN lesions and prostate cancer. Prostate. 2005;64(4):341-6.

10. Beltran H, Rickman DS, Park K, Chae SS, Sboner A, MacDonald TY, *et al*., Molecular characterization of neuroendocrine prostate cancer and identification of new drug targets. Cancer Discov. 2011;1(6):487-95.

11. Moretti L, Niermann K, Schleicher S, Giacalone NJ, Varki V, Kim KW, *et al*. MLN8054, A Small Molecule Inhibitor of Aurora Kinase A, Sensitizes Androgen-Resistant Prostate Cancer to Radiation. Int J Radiat Oncol Biol Phys. 2011;80(4):1189-97.

12. Takahashi H, Koshimizu U, Miyazaki J, Nakamura T. Impaired spermatogenic ability of testicular germ cells in mice deficient in the LIM-kinase 2 gene. Dev Biol. 2002;241(2):259-72.

13. Wang J, Nikhil K, Viccaro K, Lei C, Jacobsen M, Sandusky G, et al. Aurora A-Twist1 Axis Promotes Highly Aggressive Phenotypes in Pancreatic Carcinoma. J Cell Sci. 2017;130(6):1078-1093.

14. Sun KH, de Pablo Y, Vincent F, Johnson EO, Chavers AK, Shah K. Novel genetic tools reveal Cdk5's major role in Golgi fragmentation in Alzheimer's disease. Mol Biol Cell. 2008;19(7):3052-69.

15. Shah K, Vincent F. Divergent roles of c-Src in controlling platelet-derived growth factor-dependent signaling in fibroblasts. Mol Biol Cell. 2005;16(11):5418-32.

16. Sun KH, de Pablo Y, Vincent F, Shah K. Deregulated Cdk5 promotes oxidative stress and mitochondrial dysfunction. J Neurochem. 2008;107(1):265-78.

17. Chang KH, Multani PS, Sun KH, Vincent F, de Pablo Y, Ghosh S, et al. Nuclear envelope dispersion triggered by deregulated Cdk5 precedes neuronal death. Mol Biol Cell. 2011;22(9):1452-62.

18. Chang KH, Vincent F, Shah K*. (2012) Deregulated Cdk5 Triggers Aberrant Activation of Cell Cycle Kinases and Phosphatases Inducing Neuronal Death. *J Cell Sci* 125(Pt 21), 5124-37.

19. Shi C, Viccaro K, Lee HG, Shah K. Cdk5-FOXO3a axis: initially neuroprotective, eventually neurodegenerative in Alzheimer's disease models. J Cell Sci. 2016;129:1815-1830.

20. Wang J, Nikhil K, Viccaro K, Lei C, White J, Shah K. Phosphorylation-dependent Regulation of ALDH1A1 by Aurora Kinase A: Insights on their Synergistic Relationship in Pancreatic Cancer. BMC Biology 2017;15(1):1-10.

21. Johnson EO, Chang KH, de Pablo Y, Ghosh S, Mehta R, Badve S, et al. PHLDA1 is a crucial negative regulator and effector of Aurora A kinase in breast cancer. J Cell Sci. 2011;124(Pt 16):2711-22.

22. Sun KH, Lee HG, Smith MA, Shah, K. Direct and Indirect Roles of Cdk5 as an Upstream Regulator in the JNK Cascade: Relevance to Neurotoxic Insults in Alzheimer's Disease. Mol Biol Cell 2009;20(21):4611-9.

23. Nikhil K, Viccaro K, Shah K*. (2018) Multifaceted Regulation of ALDH1A1 by Cdk5 in Alzheimer's disease. *Mol Neurobiol*. doi: 10.1007/s12035-018-1114-9. [Epub ahead of print]

24. Nikhil K, Shah K*. (2017) The Cdk5-Mcl-1 axis promotes mitochondrial dysfunction and neurodegeneration in a model of Alzheimer's disease. *J Cell Sci*. 130(18), 3023-3039.

25. Adler HL, McCurdy MA, Kattan MW, Timme TL, Scardino PT, Thompson TC. Elevated levels of circulating interleukin-6 and transforming growth factor-beta1 in patients with metastatic prostatic carcinoma. J Urol 1999;161:182–7

26. Wise GJ, Marella VK, Talluri G, Shirazian D. Cytokine variations in patients with hormone treated prostate cancer. J Urol 2000;164:722–5

27. Shabsigh A, Ghafar MA, de la Taille A, Burchardt M, Kaplan SA, Anastasiadis AG, et al. Biomarker analysis demonstrates a hypoxic environment in the castrated rat ventral prostate gland. J Cell Biochem 2001;81(3):437-44.

28. Shabsigh A, Chang DT, Heitjan DF, Kiss A, Olsson CA, Puchner PJ, et al. Rapid reduction in blood flow to the rat ventral prostate gland after castration: preliminary evidence that androgens influence prostate size by regulating blood flow to the prostate gland and prostatic endothelial cell survival. Prostate. 1998;36(3):201-6.

29. Häggström S, Wikström P, Bergh A, Damber JE. Expression of vascular endothelial growth factor and its receptors in the rat ventral prostate and Dunning R3327 PAP adenocarcinoma before and after castration. Prostate. 1998;36(2):71-9.

30. Johansson A, Rudolfsson SH, Wikström P, Bergh A. Altered levels of angiopoietin 1 and tie 2 are associated with androgen-regulated vascular regression and growth in the ventral prostate in adult mice and rats. Endocrinology. 2005;146(8):3463-70.

31. Wu D, Yotnda P. Induction and testing of hypoxia in cell culture. J Vis Exp. 2011:(54). pii: 2899. doi: 10.3791/2899.

32. Gort EH, van Haaften G, Verlaan I, Groot AJ, Plasterk RH, Shvarts A, et al. (2008) The TWIST1 oncogene is a direct target of hypoxia-inducible factor-2alpha. Oncogene 2008;27(11):1501-10.

33. Fellmann C, Hoffmann T, Sridhar V, Hopfgartner B, Muhar M, Roth M et al. An optimized microRNA backbone for effective single-copy RNAi. Cell Rep. 2013;5(6):1704-13.

34. Lagoutte E, Villeneuve C, Lafanechère L, Wells CM, Jones GE, Chavrier P, et al. (2016) LIMK Regulates Tumor-Cell Invasion and Matrix Degradation Through Tyrosine Phosphorylation of MT1-MMP. Sci Rep 2016;6:24925.

35. Shiota M, Yokomizo A, Tada Y, Inokuchi J, Kashiwagi E, Masubuchi D, et al. Castration resistance of prostate cancer cells caused by castration-induced oxidative stress through Twist1 and androgen receptor overexpression. Oncogene 2010;29(2): 237–250.

36. Shiota M, Kashiwagi E, Yokomizo A, Takeuchi A, Dejima T, Song Y, et al. (2013) Interaction between docetaxel resistance and castration resistance in prostate cancer: Implications of Twist1, YB-1, and androgen receptor. Prostate 2013;73(12):1336-44.

37. Bose R, Holbert MA, Pickin KA, Cole PA. Protein tyrosine kinase-substrate interactions. Curr Opin Struct Biol 2006;16(6):668-75.

38. Goldsmith EJ, Akella R, Min X, Zhou T, Humphreys JM. Substrate and docking interactions in serine/threonine protein kinases. Chem Rev. 2007;107(11):5065-81.

39. Hamill S, Lou HJ, Turk BE, Boggon TJ. Structural Basis for Noncanonical Substrate Recognition of Cofilin/ADF Proteins by LIM Kinases. Mol Cell 2016;62(3):397-408.

40. Mezna M, Wong AC, Ainger M, Scott RW, Hammonds T, Olson MF. Development of a high-throughput screening method for LIM kinase-1 using a luciferase-based assay of ATP consumption. J Biomol Screen 2012;17(4):460-8.

41. Li P, Yang R, Gao W-Q. Contributions of epithelial-mesenchymal transition and cancer stem cells to the development of castration resistance of prostate cancer. Mol Cancer. 2014;13:55.

42. Schmalhofer O, Brabletz S, Brabletz T. (2009) E-cadherin β-catenin, and ZEB1 in malignant progression of cancer. Cancer Metastasis Reviews 2009;28:151–166.

43. Zeisberg M, Neilson EG. Biomarkers for epithelial-mesenchymal transitions. Journal of Clinical Investigation 2009;119:1429–1437.

44. Goodwin NC, Cianchetta G, Burgoon HA, Healy J, Mabon R, Strobel ED, Allen J, Wang, Hamman BD, Rawlins DB. (2014) Discovery of a Type III Inhibitor of LIM Kinase 2 That Binds in a DFG-Out Conformation. ACS Med Chem Lett. 2014;6(1):53-7.

45. Rak R, Haklai R, Elad-Tzfadia G, Wolfson HJ, Carmeli S, Kloog Y. (2014) Novel LIMK2 Inhibitor Blocks Panc-1 Tumor Growth in a mouse xenograft model. Oncoscience 2014;1(1):39-48.

46. Petrilli A, Copik A, Posadas M, Chang LS, Welling DB, Giovannini M, Fernández-Valle C. LIM domain kinases as potential therapeutic targets for neurofibromatosis type 2. Oncogene 2014;33(27):3571-82.

47. Li R, Doherty J, Antonipillai J, Chen S, Devlin M, Visser K, et al. (2013) LIM kinase inhibition reduces breast cancer growth and invasiveness but systemic inhibition does not reduce metastasis in mice. Clin Exp Metastasis. 2013;30(4):483-95.

48. Wang S, Ren T, Jiao G, Huang Y, Bao X, Zhang F, Liu K, Zheng B, Sun K, Guo W. (2017) BMPR2 promotes invasion and metastasis via the RhoA-ROCK-LIMK2 pathway in human osteosarcoma cells. Oncotarget 2017;8(35):58625-58641.

49. Aggelou H, Chadla P, Nikou S, Karteri S, Maroulis I, Kalofonos HP, et al. LIMK/cofilin pathway and Slingshot are implicated in human colorectal cancer progression and chemoresistance. Virchows Arch. 2018;472(5):727-737.

50. Vardouli L, Moustakas A, Stournaras C. LIM-kinase 2 and cofilin phosphorylation mediate actin cytoskeleton reorganization induced by transforming growth factor-beta. J Biol Chem. 2005;280(12):11448-57.

51. Niu Y, Ma F, Huang W, Fang S, Li M, Wei T, Guo L. Long non-coding RNA TUG1 is involved in cell growth and chemoresistance of small cell lung cancer by regulating LIMK2b via EZH2. Mol Cancer 2017;16(1):5.

52. Hoang DT, Iczkowski KA, Kilari D, See W, Nevalainen MT. Androgen receptor-dependent and -independent mechanisms driving prostate cancer progression: Opportunities for therapeutic targeting from multiple angles. Oncotarget 2017;8(2):3724-3745.

53. Yamasaki M, Nomura T, Sato F, Mimata H. Chronic hypoxia induces androgen-independent and invasive behavior in LNCaP human prostate cancer cells. Urol Oncol [Internet]. Elsevier Inc.; 2013;31:1124–31.

54. Semenza GL. Hypoxia-inducible factors in physiology and medicine. Cell 2012;148:399–408.

55. Stewart GD, Ross JA, McLaren DB, Parker CC, Habib FK, Riddick AC. The relevance of a hypoxic tumour microenvironment in prostate cancer. BJU Int 2010;105:8–13.

56. Fernandez EV, Reece KM, Ley AM, Troutman SM, Sissung TM, Price DK, et al. (2015) Dual targeting of the androgen receptor and hypoxia-inducible factor 1α pathways synergistically inhibits castration-resistant prostate cancer cells. Mol Pharmacol. 2015;87(6):1006-12.

57. Mizukami T, Kamachi H, Mitsuhashi T, Tsuruga Y, Hatanaka Y, Kamiyama T, et al. Immunohistochemical analysis of cancer stem cell markers in pancreatic adenocarcinoma patients after neoadjuvant chemoradiotherapy. BMC Cancer 2014;14:687.

58. Shiota M, Song Y, Takeuchi A, Yokomizo A, Kashiwagi E, Kuroiwa K, et al. Antioxidant therapy alleviates oxidative stress by androgen deprivation and prevents conversion from androgen dependent to castration resistant prostate cancer. J Urol 2012;187(2):707–714.

59. Shiota M, Kashiwagi E, Yokomizo A, Takeuchi A, Dejima T, Song Y, et al. Interaction between docetaxel resistance and castration resistance in prostate cancer: Implications of Twist1, YB-1, and androgen receptor. Prostate. 2013;73(12):1336-44.

60. Shiota M, Itsumi M, Takeuchi A, Imada K, Yokomizo A, Kuruma H, et al. Crosstalk between epithelial-mesenchymal transition and castration resistance mediated by Twist1/AR signaling in prostate cancer. Endocr Relat Cancer 2015;22(6):889-900.

61. Moffat J, Grueneberg DA, Yang X, Kim SY, Kloepfer AM, Hinkle G, et al. (2006) A lentiviral RNAi library for human and mouse genes applied to an arrayed viral high-content screen. Cell. 2006;124(6):1283-98.

62. Wiederschain D, Wee S, Chen L, Loo A, Yang G, Huang A. Single-vector inducible lentiviral RNAi system for oncology target validation. Cell Cycle. 2009;8(3):498-504.

63. Sanjana NE, Shalem O, Zhang F. Improved vectors and genome-wide libraries for CRISPR screening. Nat Methods. 2014;11(8):783-4.

Figure legends:

Figure 1: (A) LIMK2 levels increase upon castration in mice prostate. LIMK2 and IL6 levels were analyzed in C57BL/6N mice post-castration (day 0, 3, 5, 7). Three mice were included in each group. (B) Relative protein levels of LIMK2 (ratio of LIMK2/actin) and IL6 (ratio of IL6/actin) from castrated mice on different days. The data shown are mean ± SEM of three independent experiments. (C) LIMK2 levels were analyzed using IHC in mouse prostates isolated on different days following castration. (D) LIMK2 and TWIST1 levels were upregulated when C4-2 cells were treated with 100 µM cobalt chloride for 24 h. LIMK2 and TWIST1 levels represent the ratios of (LIMK2 or TWIST1)/Actin. (E) LIMK2 and TWIST1 levels in C4-2 cells treated with cobalt chloride. The data shown are mean ± SEM of three independent experiments. *P <0.05 compared to control cells. (F) LIMK2 and TWIST1 are upregulated in hypoxia-exposed C4-2 cells treated for 12h and 18h. LIMK2 and TWIST1 levels represent the ratios of (LIMK2 or TWIST1)/Actin. (G) LIMK2 and TWIST1 protein levels in hypoxia-induced C4-2 cells. Data shown are mean ± SEM of three independent experiments. *P <0.05 compared to control cells. (H) LIMK2 and TWIST1 mRNA levels increase in hypoxia-exposed C4-2 cells as analyzed by qPCR. (I) Increase in LIMK2 promoter activity following 12h and 24h of cobalt chloride exposure. Four different LIMK2 promoter fused to luciferase were created. 360, 600, 900 and 1038 are upstream positions from the start site for LIMK2. (J) LIMK2 promoter is activated upon hypoxia as tested by 4 different LIMK2-luciferase plasmids. (K) LIMK2 levels do not change upon androgen depletion in LNCaP cells. The cells were treated with charcoal-stripped media for 12h, and LIMK2 levels analyzed. (E) Bar graph showing LIMK2 levels under normal and androgen depleted media. The data shown are mean ± SEM of six independent experiments.

Figure 2: LIMK2 regulates TWIST1 levels. (A) LIMK2 ablation using specific shRNA decrease TWIST1 mRNA levels under hypoxic conditions (12h and 18h). LIMK2 and TWIST1 mRNA levels were measured using qPCR. (B) LIMK2 ablation using specific shRNA decrease TWIST1 protein levels under hypoxic and normoxic conditions. (C) LIMK2 and TWIST1 protein levels in control and LIMK2-shRNA treated cells. Data shown are mean ± SEM of three independent experiments. *P <0.05 compared to control cells and $^{\#}$P <0.05 compared to hypoxic cells. (D) TWIST1 mRNA levels in LIMK2-CRISPR C4-2 cells under normoxic and hypoxic conditions (12h and 18h treatments), measured using qPCR. (E) TWIST1 protein levels in LIMK2-CRISPR C4-2 cells under normoxic and hypoxic conditions. (F) TWIST1 protein levels in LIMK2-CRISPR C4-2 cells under normoxic and hypoxic conditions. Data shown are mean ± SEM of three independent experiments. *P <0.05 compared to control cells and $^{\#}$P <0.05 compared to hypoxic cells. (G) TWIST1 does not regulate LIMK2 mRNA levels. LIMK2 mRNA levels in TWIST1 shRNA treated C4-2 cells under normoxic and hypoxic conditions. (H) TWIST1 ablation decreases LIMK2 protein levels under normoxic conditions, but not under hypoxic conditions. (I) TWIST1 ablation decreases LIMK2 levels under normoxic conditions, but not under hypoxic conditions. Data shown are mean ± SEM of three independent experiments. *P <0.05 compared to control cells and $^{\#}$P <0.05 compared to hypoxic cells.

Figure 3: LIMK2 levels increase with prostate cancer progression with highest levels in CRPC clinical specimens. (A) Immunohistochemical micrographs representing LIMK2 specificity in normal prostate, stages II and III prostate cancer, and castration resistant prostate cancer with annotations of staining localization. All images are at 40x magnification. (B) C4-2 cells were

stably transfected with pTet-pLKO-LIMK2 shRNA and miR-LIMK2 shRNA, which encodes a doxycycline (Dox)-inducible LIMK2shRNA. The stable cells were generated in which endogenous LIMK2 levels could be downregulated by treatment with doxycycline. The figure shows LIMK2 downregulation in these stable cells after 72h of doxycycline treatment. (C) C4-2-pTet-pLKO-LIMK2 shRNA and C4-2-miR-LIMK2 shRNA cells were injected subcutaneously into the flank region of castrated nude mice (n = 3 in each group). The mice were fed with normal diet and water until subcutaneous tumors reached an average volume of ~1500 mm^3. The mice were supplied with doxycycline in drinking water. Tumor volumes were measured twice a week until 45 days post injection. (D) Representative images of mice bearing tumors taken 45 days after injection. (E) Gross images of dissected tumors.

Figure 4: TWIST1 is a direct substrate of LIMK2. (A) TWIST1 is directly phosphorylated by LIMK2. Lane 1 contains [^{32}P]ATP and LIMK2, lane 2 contains 6x-His-TWIST1, LIMK2 and [^{32}P]ATP, and lane 3 contains 6x-His-TWIST1 with [^{32}P]ATP. Kinase assay was conducted for 15 minutes. The lower panel shows LIMK2 and TWIST1 ponceau stain. (B) LIMK2 phosphorylates TWIST1 at S45, S78, S95 and S199. The corresponding phospho-resistant single mutants (S45A, S78A, S95A and S199A) were generated and subjected to *in vitro* kinase assay using LIMK2. The top panel shows autoradiography, second panel shows TWIST1 ponceau stain, and third panel shows LIMK2 ponceau stain. (C) Bar graph showing the phospho-levels of WT and phospho-resistant single mutants of TWIST1. (D) LIMK2 only phosphorylates TWIST1 at these 4 sites (S45, S78, S95 and S199), as the corresponding 4A- phospho-resistant mutant shows no phosphorylation, when subjected to in vitro kinase assay with LIMK2. (E) Subcellular localization of TWIST1 in C4-2 cells treated with scrambled or LIMK2 shRNA for 30 h. (F) 4A-

mutant shows similar subcellular localization as wild-type TWIST1. HA-tagged 4A-TWIST1 was expressed in C4-2 cells and its subcellular localization was analyzed using HA antibody. (G) Subcellular localization of WT and 4A TWIST1 mutant in C4-2 cells. (H) Subcellular fractionation of TWIST1 in C42, LIMK2-CRISPR C4-2 and LIMK2 shRNA-treated C4-2 cells. Alpha-tubulin is the cytoplasmic marker and lamin A is the nuclear marker. N, nuclear fraction; C, cytoplasmic fraction.

Figure 5: LIMK2 positively regulates TWIST1 protein levels. (A) LIMK2 overexpression increases TWIST1 levels in C4-2 cells. LIMK2 and TWIST1 levels were analyzed in WT HA–LIMK2-expressing C4-2 and vector infected cells. (B) Histogram shows relative band intensities normalized to the corresponding tubulin level. Data are expressed as fold change relative to control; values shown as mean ± SEM of three independent experiments. * and # indicate statistically significant differences with respect to controls for TWIST1 and LIMK2 proteins, respectively. $p < 0.05$ analyzed by two-way analysis of variance. (C) LIMK2 ablation depletes TWIST1 in C4-2 cells. Cells were infected with scrambled shRNA, or LIMK2-shRNA-1, -2 or -3, and LIMK2 and TWIST1 levels analyzed. (D) Histogram shows relative band intensities normalized to the corresponding tubulin level. Data shown as mean ± SEM of three independent experiment. * and # indicate statistically significant differences with respect to controls for TWIST1 and LIMK2 proteins, respectively. $p < 0.05$ analyzed by two-way analysis of variance (E) LIMK2 inhibits TWIST1 degradation. LIMK2 C4-2 and C4-2 cells were treated with cycloheximide (CHX, 10 μM) for 2h and 4h, and LIMK2 and TWIST1 levels analyzed. (F) Graphical representation of LIMK2 degradation rate in cells treated as in E. The results of densitometric scanning are shown graphically with the LIMK2 signal normalized to actin signal.

(G) Graphical representation of TWIST1 degradation rate. (H) LIMK2 stabilizes TWIST1 by inhibiting its ubiquitylation. Cells were co-transfected with LIMK2 shRNA along with 6x-His–ubiquitin (6x-His-Ub). Ubiquitylated proteins were immunoprecipitated and TWIST1 was analyzed. Each experiment was performed at least three independent times. Representative data are shown. (I) 4A-TWIST1 is less stable than WT TWIST1 in C4-2 cells. WT and 4A-TWIST1 were stably expressed in C4-2 cells and their expression analyzed. (J) TWIST1 is rapidly ubiquitylated upon LIMK2 compared to 4A-TWIST1 in C4-2 cells. (K) Levels of TWIST1 in stable cell lines expressing either WT, 4A-TWIST1 or any of the single phospho-resistant mutant. (L) Same data as Figure F, except datashown are mean ± SEM of three independent experiments. *P <0.05 compared to control cells. (M) Ubiquitylation pattern of WT and all single phospho-resistant mutant with and without LIMK2 ablation.

Figure 6: TWIST1 positively regulates LIMK2 protein levels. (A) Overexpression of WT HA-tagged TWIST1 increases LIMK2 levels in C4-2 cells. (B) Histogram shows relative band intensities normalized to the corresponding tubulin level. Data shown are mean ± SEM of three independent experiments. * and # indicate statistically significant differences with respect to controls for TWIST1 and LIMK2 proteins, respectively. $p < 0.05$ analyzed by two-way analysis of variance. (C) TWIST1 ablation depletes LIMK2 in C4-2 cells. (D) Histogram shows relative band intensities normalized to the corresponding tubulin level. Data shown as mean ± SEM of three independent experiment. (E) TWIST1 inhibits LIMK2 degradation. TWIST1-C4-2 and C4-2 cells were treated with cycloheximide (CHX) for 2 h and 4 h, and LIMK2 and TWIST1 levels analyzed. (F) Graphical representation of TWIST1 degradation rate. (G) Graphical representation

of LIMK2 degradation rate. (H) TWIST1 stabilizes LIMK2 by inhibiting its ubiquitylation. Each experiment was performed at least three independent times. Representative data are shown.

Figure 7: LIMK2-mediated TWIST1 phosphorylation contributes to aggressive oncogenic phenotypes. (A) TWIST1 promotes cell proliferation in C4-2 cells. C4-2, LIMK2-C4-2, TWIST1-C4-2, and 4A-TWIST1-C4-2 cells were plated in 96-well plates and cultured for 24, 48, and 72 h. At the end of the incubation, an MTT assay was performed. (B) LIMK2 depletion decreases cell proliferation in TWIST1-C4-2 cells, but not in phospho-resistant 4A-TWIST1-C4-2 cells. MTT assay was performed after 48h. (C) LIMK2 overexpression increases cell proliferation in TWIST1-C4-2 cells, but not in 4A- TWIST1-C4-2 cells. (D) TWIST1 promotes colony formation in a soft agar assay in C4-2 cells. *$p < 0.05$ compared to vector-expressing control analyzed by two-way analysis of variance. (E) TWIST1 promotes cell motility in C4-2 cells. Chemotaxis assay was performed in C4-2, TWIST1-C4-2 and 4A-TWIST1-C4-2 cells using Boyden chambers. These experiments were performed three independent times. Representative data are shown. Magnification, 200× (F) Histogram shows mean ± SEM of three independent experiments. **$p < 0.05$ compared to vector-expressing control analyzed by two-way analysis of variance. (G and H) LIMK2 depletion inhibits cell motility in TWIST1-C4-2 cells, but not in phospho-resistant 4A-TWIST1-C4-2 cells. (I and J) LIMK2 overexpression increases cell motility in TWIST1-C4-2 cells, but not in 4A-TWIST1-C4-2 cells. (K) TWIST1 expression increases the levels of EMT and CSC markers but decreases E-cadherin levels. 4A-TWIST1expression decreases the levels of EMT and CSC markers but increases E-cadherin. (L) TWIST1 overexpression increases the sphere-forming ability in C4-2 cells. (M) TWIST1 overexpression increases drug resistance in C4-2 cells. C4-2 cells and C4-2 cells expressing WT

TWIST1 and 4A-TWIST1, were plated in 96-well plates overnight. Doxorubicin (1 µM) was added and cells were cultured for another 24, 48 or 72 h.

Figure 8: The TWIST1–LIMK2 axis regulates EMT *in vivo*. (A) TWIST1overexpression increases tumorigenesis *in vivo*. Five male NRG-SCID mice were inoculated with C4-2 cells and TWIST1-C4-2 cells on left and right shoulder, respectively. (B) NRG-SCID mouse were injected with control C4-2 cells and TWIST1-C4-2 cells on the left and right shoulder, respectively. The pictures were taken 23 days following inoculation. A representative image is shown. (C) Effect of 4A-TWIST1 expression on subcutaneous tumor growth in athymic nude mice. Three nude mice were inoculated with TWIST1-C4-2 cells and 4A-TWIST1-C4-2 cells on the right and left shoulder, respectively. (D) Athymic nude mouse injected with TWIST1-C4-2 cells and 4A-TWIST1- C4-2 cells on right and left shoulder. The pictures were taken 23 days following inoculation. A representative image is shown. (E) Immunoblot analysis to show the expression of levels of LIMK2, EMT and CSC markers in the tumors of NRG-SCID mouse originating from control C4-2 and TWIST1-C4-2 cells. (F) Histogram shows relative band intensities normalized to the corresponding Actin level. Data shown as mean ± SEM of three independent experiments. * indicates statistically significant differences with respect to controls. $p < 0.05$ analyzed by two-way analysis of variance. (G) E-cadherin immunohistochemistry of C4-2 and TWIST1-C4-2 xenografts. (H) LIMK2 immunohistochemistry of C4-2 and TWIST1-C4-2 xenografts. (I) MMP2 immunohistochemistry of C4-2 and TWIST1-C4-2 xenografts. (J) CD44 immunohistochemistry of C4-2 and TWIST1-C4-2 xenografts. (K) Snail immunohistochemistry of C4-2 and TWIST1-C4-2 xenografts. (L) Slug immunohistochemistry of C4-2 and TWIST1-C4-2 xenografts. (M) Pre-treatment with 10 nM Docetaxel followed by 10 µM LIMK2 inhibitor

for next 48 h sensitizes C4-2 cells to docetaxel-induced cell death. Combination Index generated using CompuSyn software.

Data shown are mean ± SEM of three independent experiments. *P <0.05 compared to control cells. (N) Our model showing the contribution of LIMK2 and TWIST1 in CRPC progression and aggressive phenotypes.

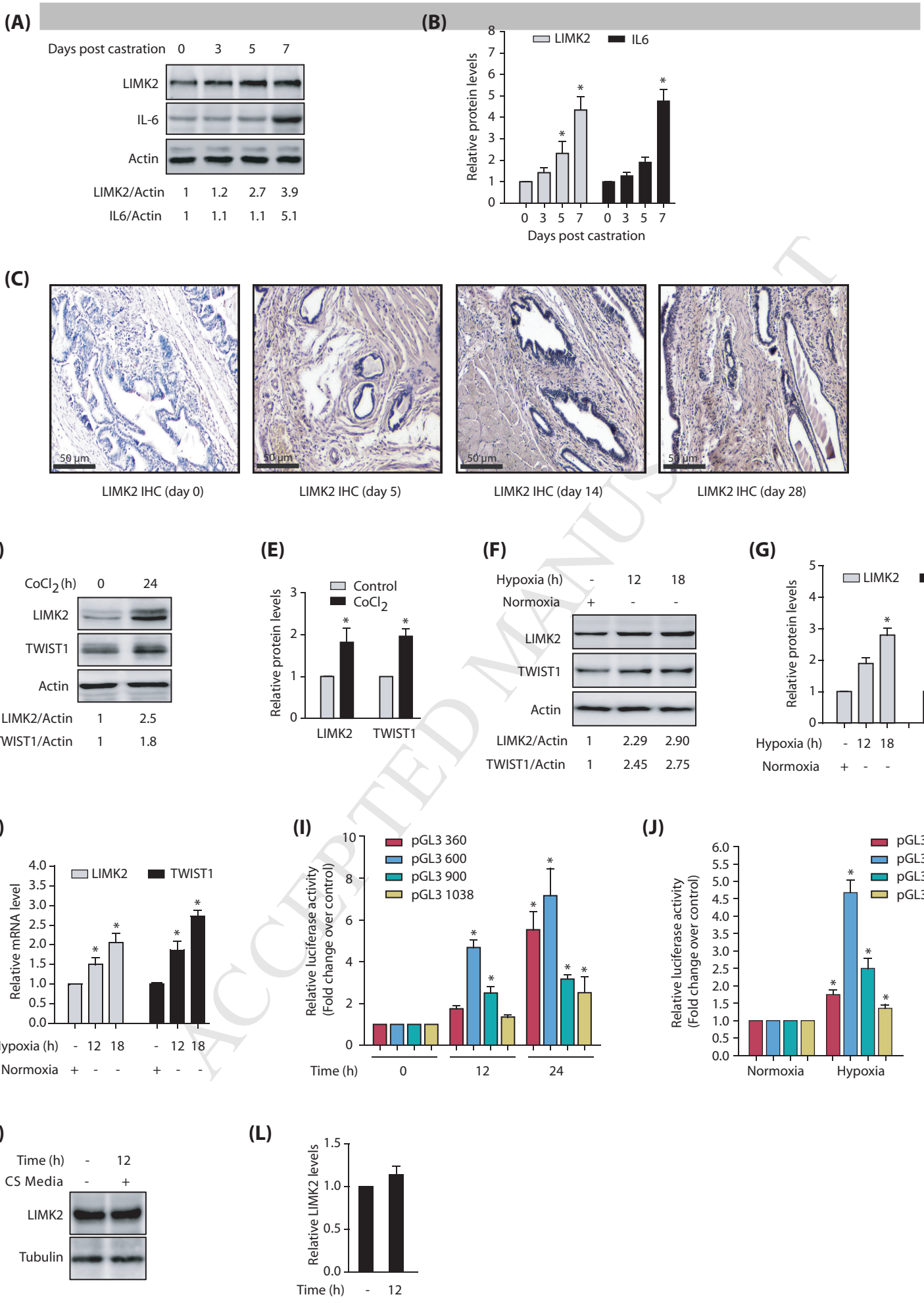

Figure 1

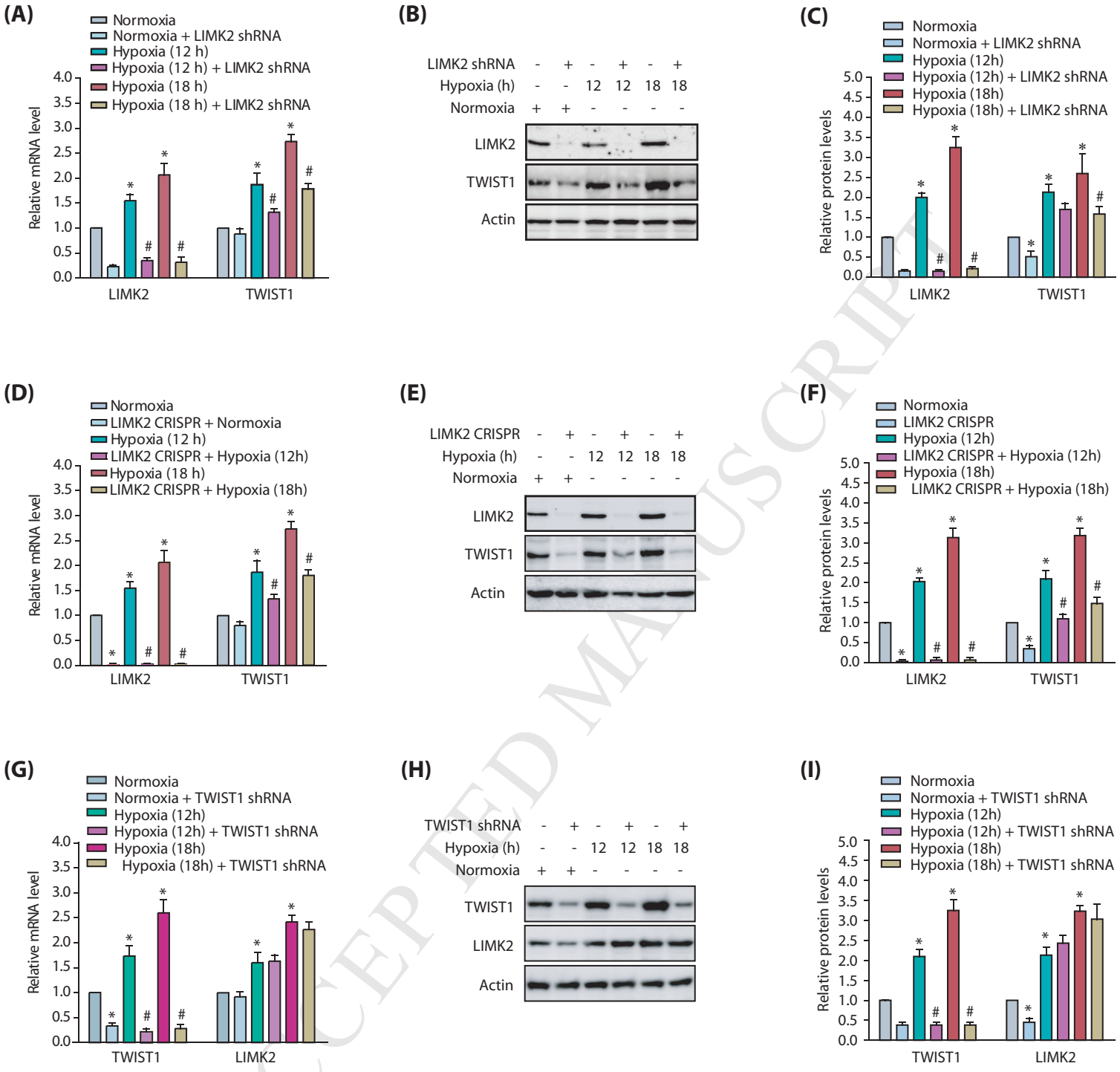

Figure 2

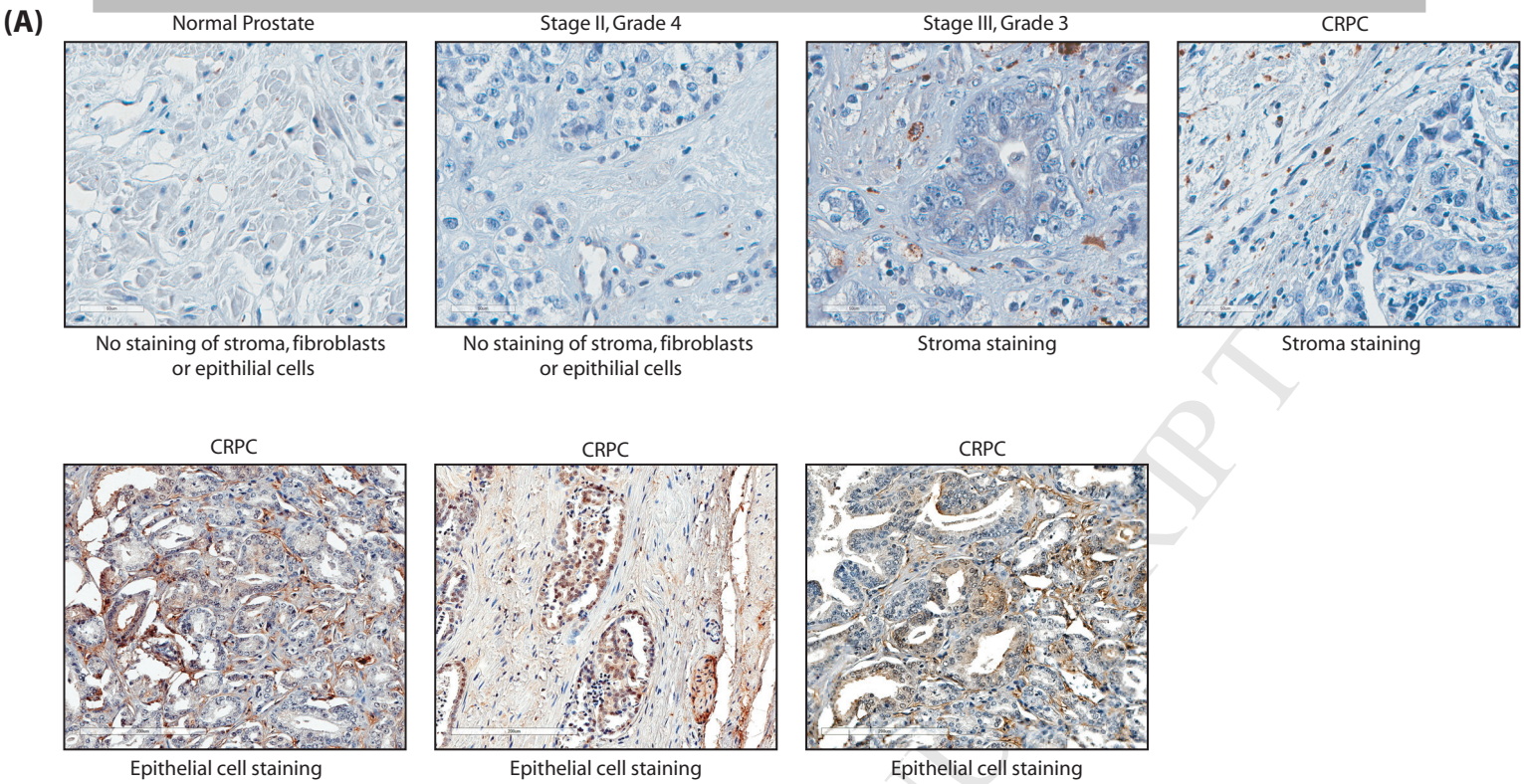

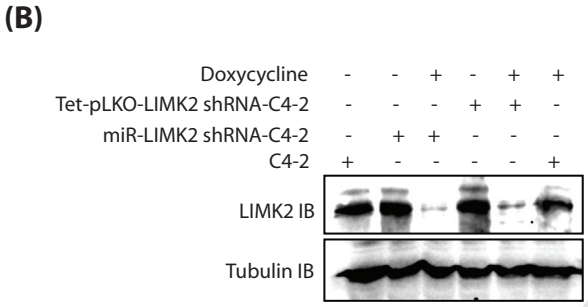

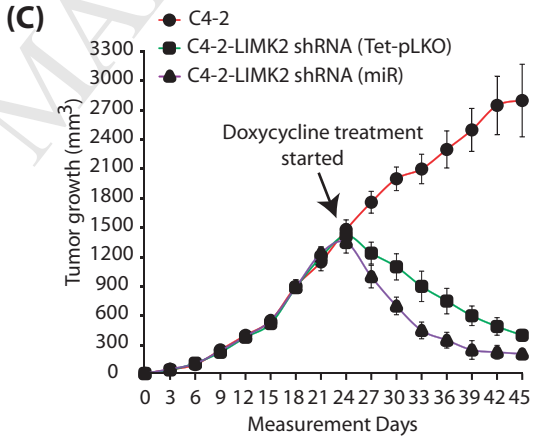

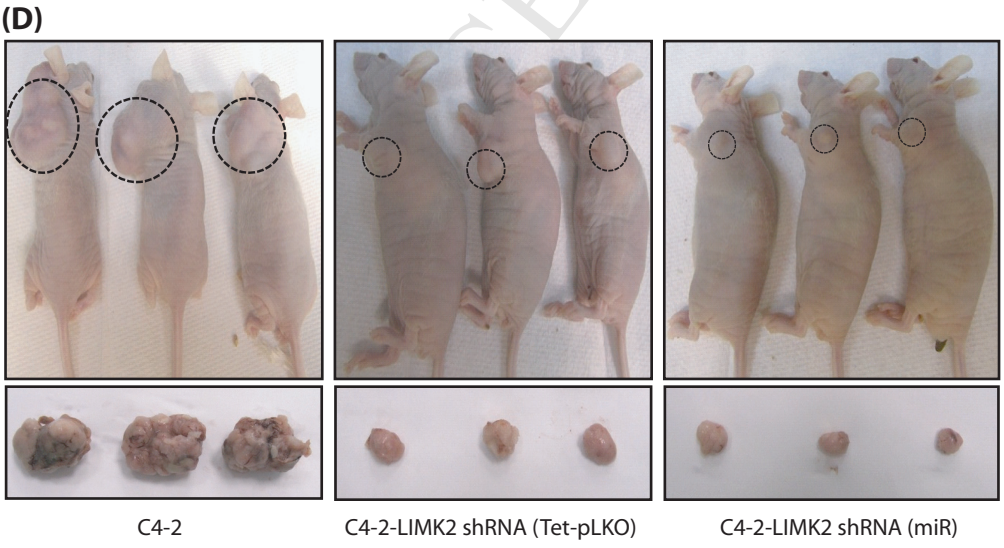

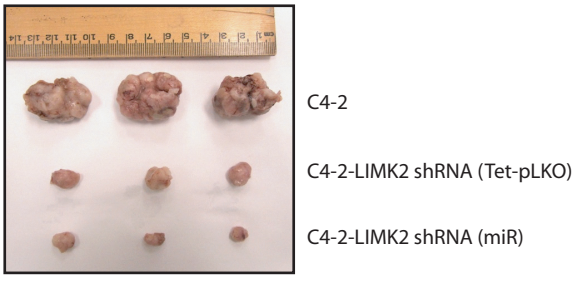

Figure 3

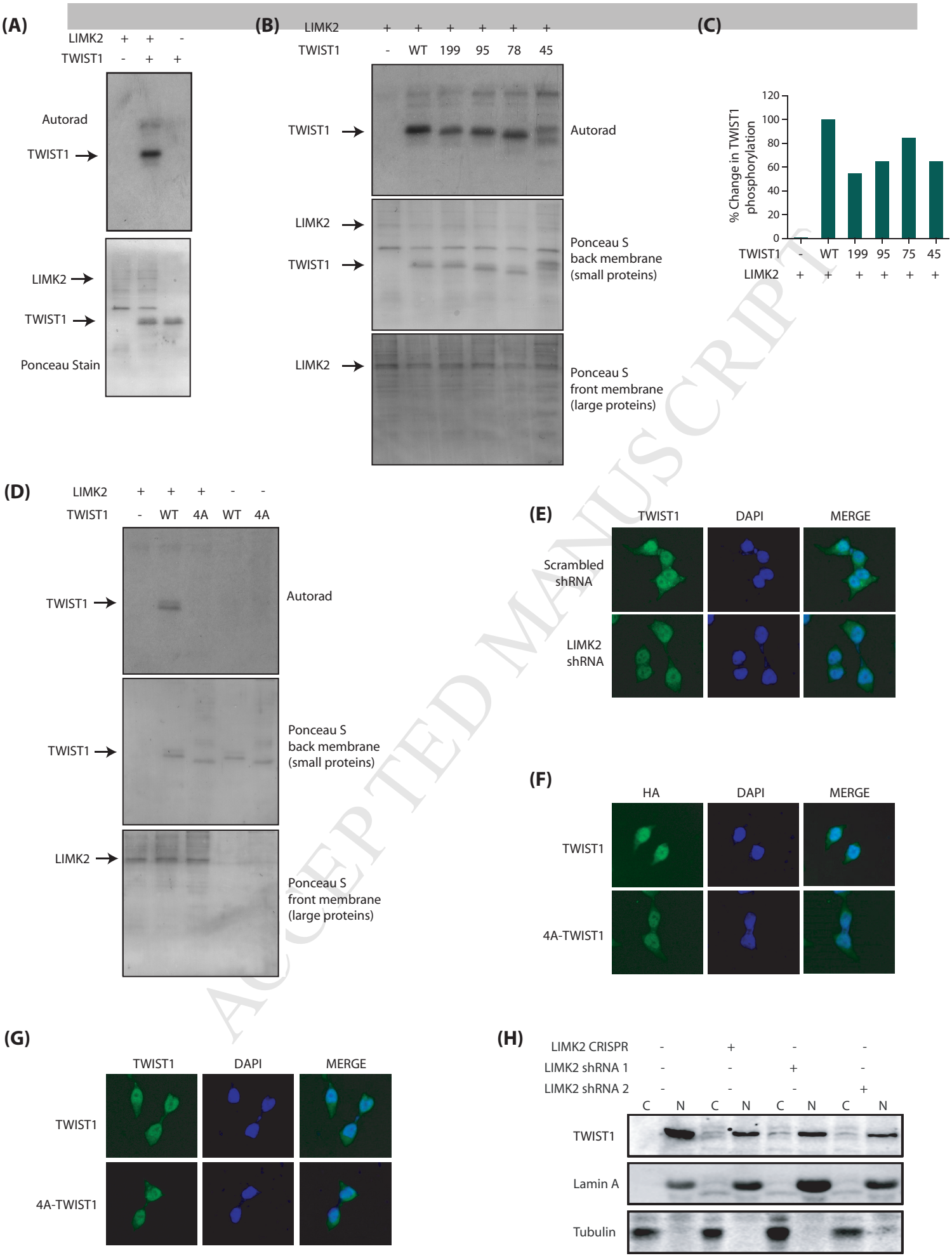

Figure 4

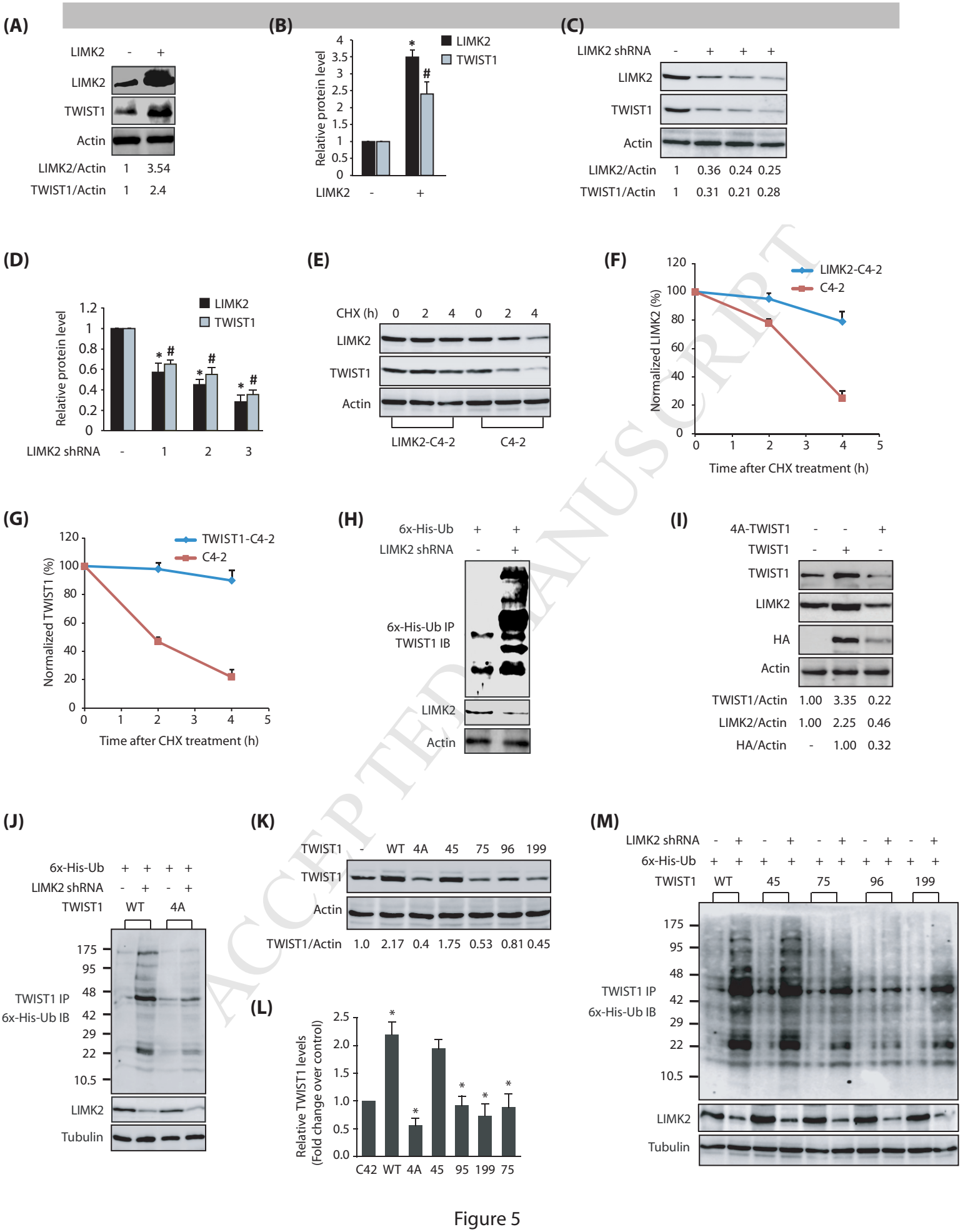

Figure 5

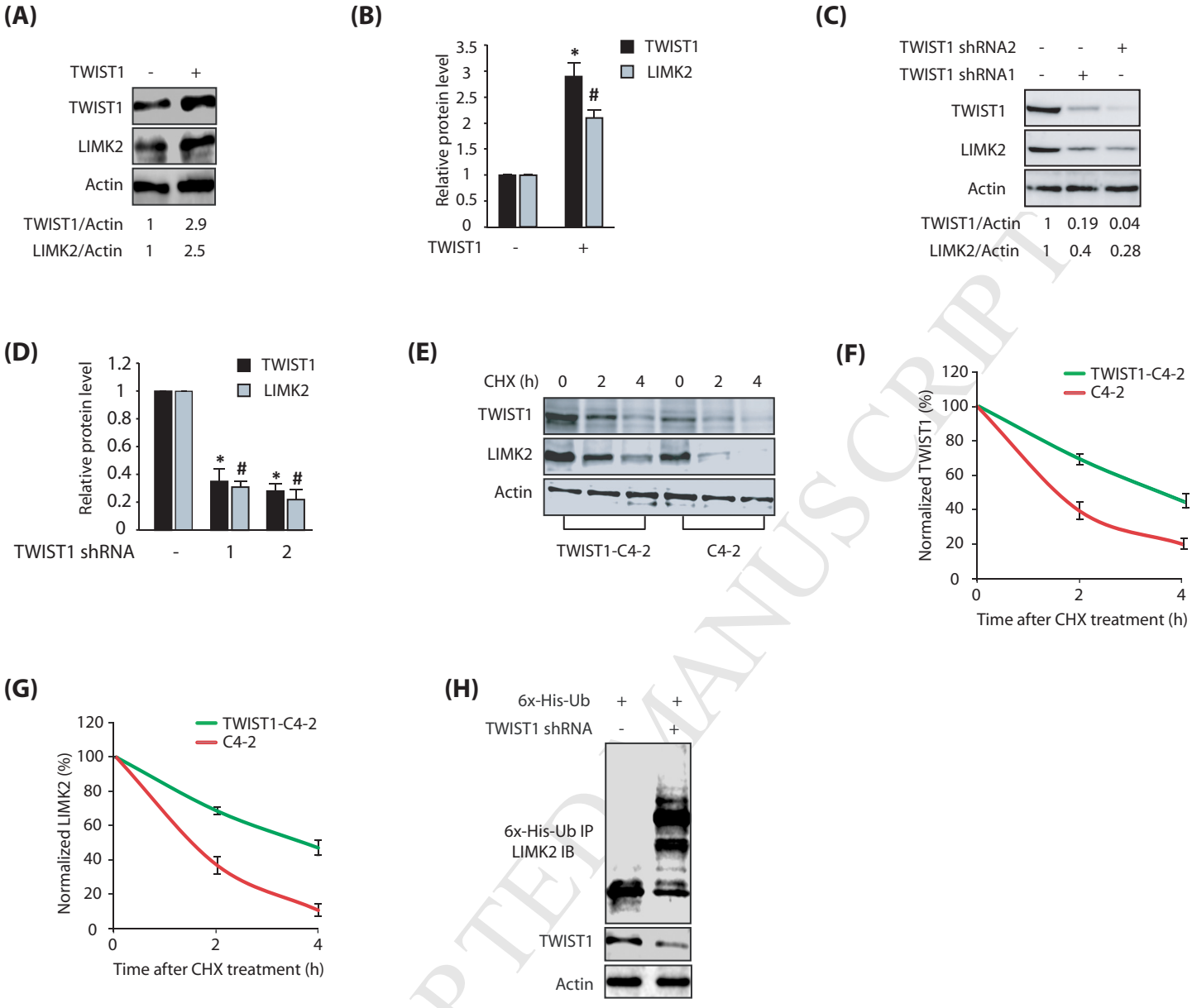

Figure 6

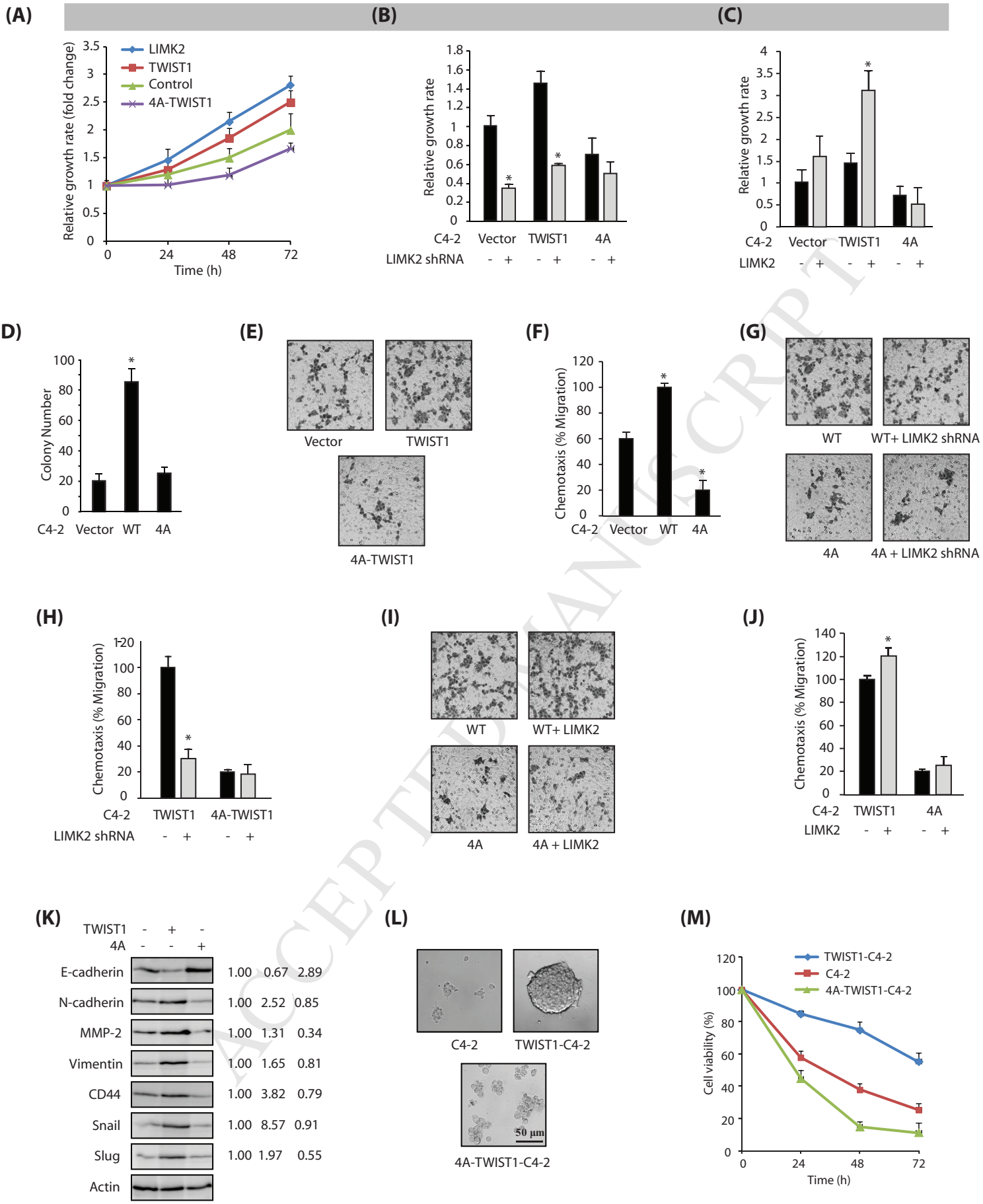

Figure 7

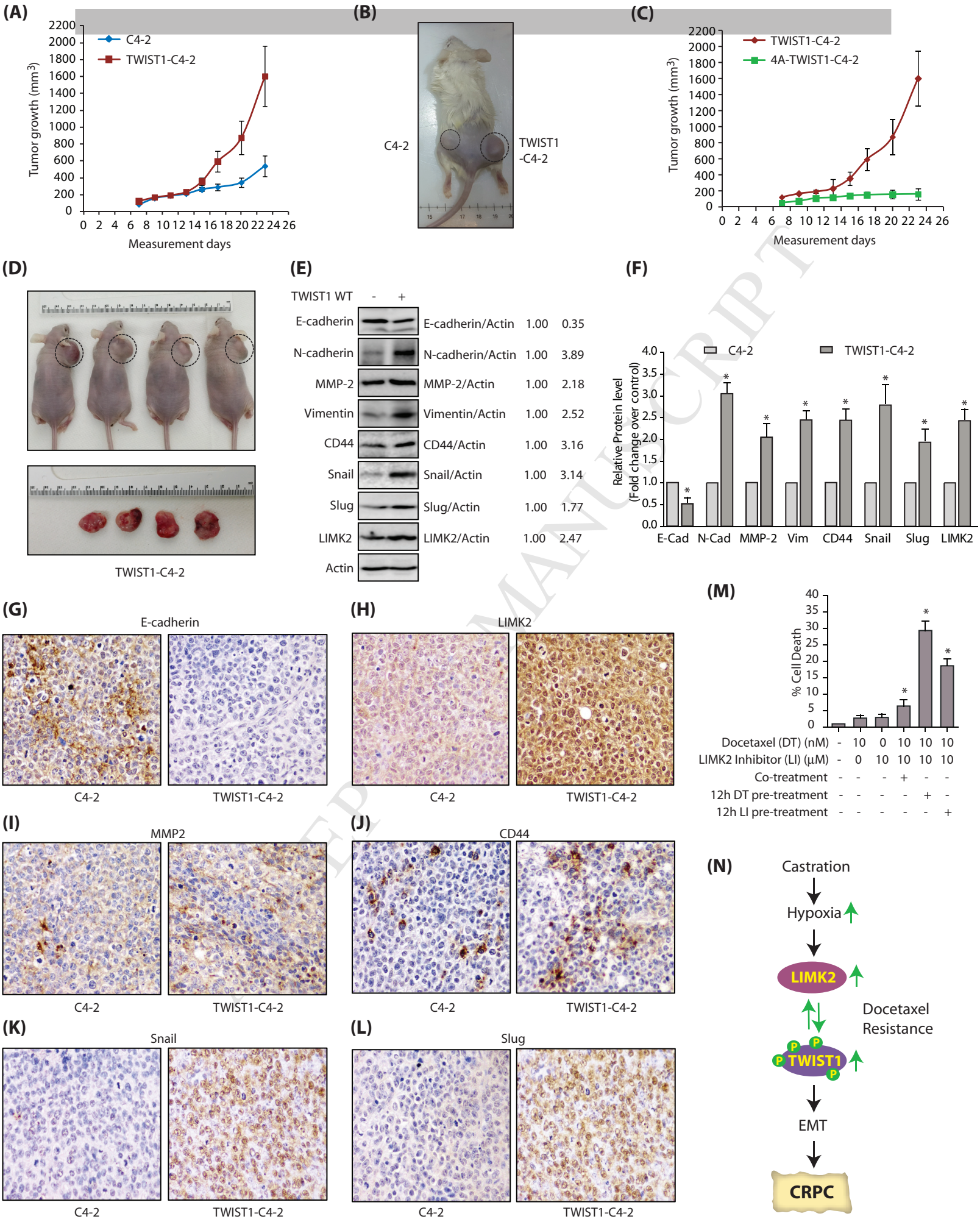

Figure 8

Highlights:

• LIMK2 was identified as a disease-specific target in CRPC.

• We show that LIMK2 is upregulated in castrated prostates due to increased hypoxia.

• Inducible knockdown of LIMK2 fully reverses CRPC tumorigenesis in castrated mice.

• TWIST1 was identified a direct target of LIMK2.

• LIMK2 inhibitor shows very high synergy with docetaxel.

The authors declare no conflict of interest.